Single-coil properties and concentration effects for polyelectrolyte-like wormlike micelles: a Monte Carlo study

2002 J. Phys.: Condens. Matter 14 2283

(http://iopscience.iop.org/0953-8984/14/9/317)

INSTITUTE OF PHYSICS PUBLISHING JOURNAL OF PHYSICS: CONDENSED MATTER

J. Phys.: Condens. Matter **14** (2002) 2283–2295 PII: S0953-8984(02)31170-6

Single-coil properties and concentration effects for polyelectrolyte-like wormlike micelles: a Monte Carlo study

Luigi Cannavacciuolo[1], **Jan Skov Pedersen**[2] **and Peter Schurtenberger**[3]

[1] Institut für Polymere, Eidgenössische Technische Hochschule, CH-8092 Zürich, Switzerland
[2] Department of Chemistry, University of Aarhus, DK-4000 Aarhus, Denmark
[3] Department of Physics, University of Fribourg, CH-1700 Fribourg, Switzerland

Received 23 November 2001
Published 22 February 2002
Online at stacks.iop.org/JPhysCM/14/2283

Abstract

Results of an extensive Monte Carlo (MC) study on both single and many semiflexible charged chains with excluded volume (EV) are summarized. The model employed has been tailored to mimic wormlike micelles in solution. Simulations have been performed at different ionic strengths of added salt, charge densities, chain lengths and volume fractions Φ, covering the dilute to concentrated regime. At infinite dilution the scattering functions can be fitted by the same fitting functions as for uncharged semiflexible chains with EV, provided that an electrostatic contribution b_{el} is added to the bare Kuhn length. The scaling of b_{el} is found to be more complex than the Odijk–Skolnick–Fixman predictions, and qualitatively compatible with more recent variational calculations. Universality in the scaling of the radius of gyration is found if all lengths are rescaled by the total Kuhn length. At finite concentrations, the simple model used is able to reproduce the structural peak in the scattering function $S(q)$ observed in many experiments, as well as other properties of polyelectrolytes (PELs) in solution. Universal behaviour of the forward scattering $S(0)$ is established after a rescaling of Φ. MC data are found to be in very good agreement with experimental scattering measurements with *equilibrium PELs*, which are giant wormlike micelles formed in mixtures of nonionic and ionic surfactants in dilute aqueous solution, with added salt.

1. Introduction

In the last decade considerable interest has been devoted to the study of wormlike micelles as an ideal model system for polyelectrolytes (PELs) [1–5]. The stronger scattering power of micellar solutions compared with conventional PELs allows one to explore the very dilute regime and to extrapolate to single-coil properties. The goal is to provide high-quality experimental

data that can be compared with existing theories to test the validity of the fundamental assumptions and approximations, which is still a matter of controversy. From a practical point of view it is relatively easy to tune a given charge density on micelles by 'doping' solutions containing giant wormlike micelles with a small amount of ionic surfactants. The resulting electrostatic interactions can be screened out by adding salt. It has been argued that such solutions exhibit static properties similar to PELs in solutions under analogous conditions [2, 4, 5]. There are, however, important differences that should be considered. Micelles are *living structures*, they can break and recombine, and the resulting molecular weight distribution is not quenched. Moreover, on increasing concentration, micelles grow and the molecular weight becomes a function of the volume fraction Φ. The exact form of the growth law is still not known, and this paper tries to take an important step also in clarifying this point (see section 4.3). Finally, micelles are believed to have a broad size distribution [1]. In our simulations we have concentrated on monodisperse systems. For long chains, polydispersity should cause no significant effect on local quantities such as the Kuhn length b. However, it is not clear whether the neglect of polydispersity is important for global quantities such as the forward scattering intensity $S(0)$. For classical PELs, a comparison between experimental data and simulation results for $S(0)$ would clearly require the incorporation of polydispersity. However, for micelles, which do possess a finite lifetime and can then considered as 'equilibrium' or 'living' polymers or PELs, it has been argued that the average mass or aggregation number is the only relevant quantity, and that the explicit form of the size distribution does not enter.

The approach to PELs in solution is particularly challenging for theories and experiments [6]. This is mainly due to two fundamental features of PELs: the long-range nature of the Coulomb interactions, and the influence not only of the solvent, as in the case of uncharged polymers, but also of counterions, and added salt ions.

Due to electrostatic repulsion charged chains are swollen compared with uncharged, and so the overlap concentration is expected to be shifted towards lower values. It usually happens that the corresponding dilute regime falls well below the detection sensitivity of the currently available scattering instruments. This makes it almost impossible to determine the structure of PELs in the dilute regime where true single-chain properties are probed. This problem is particularly relevant considering that most of the theoretical works deal with approximations valid only in this regime. In contrast, in the case of wormlike micelles all length scales are increased by a factor of five to ten, resulting a larger accessible regime for measurements.

A powerful tool to manage the specific problems posed by PELs turned out to be Monte Carlo (MC) simulations, which have already extensively and successfully been applied to uncharged polymers. PEL simulations are, however, more difficult and expensive in CPU time compared with neutral polymers. Despite the difficulties, several works have appeared in the literature in the last decades. Single chains in salt solution have been simulated both without explicit inclusion of counterions and coions [7–13], and with their inclusion (primitive model) [14]. Stevens and Kremer have performed molecular dynamics simulations of many chain systems using a *continuum model* in the Debye–Hückel approximation [15] and also including the full Coulomb interactions between monomers and counterions [16–20]. Even if progress has been made, it is still modest, and the knowledge of the fundamental issues still lacking [21]. The major efforts in the simulation research have focused on the conformational properties and on the important issue of universality. Very few studies have been devoted to analysing the scattering function of such systems. This function seems to us to deserve more attention considering that most of the experimental studies on PELs use scattering experiments where the scattering function is the directly measured quantity. With this work we have also tried to fill this gap by performing systematic and extensive MC simulations of both single- and many-charged-chain systems with excluded volume (EV). In order to achieve an exhaustive set

of results, in accordance with the large variety of possible conditions for PELs in solution, we have simulated systems at various volume fractions Φ, ionic strengths I, charge densities Z_b and chain lengths L. To better understand the effects of electrostatic interactions, uncharged chains have been simulated as well, at the same volume fractions. A further factor which has motivated us to produce a quite complete set of simulations is the idea of ending up with a full parametrization of the scattering function, as already achieved for uncharged systems [22,23], thus providing a fundamental model to analyse experimental scattering data.

Simulation data have also been compared with SANS experiments on a system consisting of a mixture of hexa-ethylene glycol mono n-hexadecyl-ether ($C_{16}E_6$) and a small amount of the ionic surfactant 1-hexadecane sulfonic acid ($C_{16}SO_3Na$), with added salt (NaCl), which gives rise to charged PEL-like micelles [5].

2. Model and simulation technique

In order to account for the semiflexibility of the wormlike micelles we have employed a discrete representation of the wormlike chain (WLC) model, introduced by Kratky and Porod [24]. It consists of a freely rotating chain of N points linked by bonds of length a, and equal valence angle θ. The chain length is therefore $L = (N-1)a$ and the intrinsic Kuhn length b is given by

$$b = a\,\frac{1+\cos\,\theta}{1-\cos\,\theta}. \tag{1}$$

EV effects are reproduced by replacing the N points on the chain with N hard spheres of radius $\rho = 0.1b$ and, when sampling, discarding those chain configurations with overlap of the spheres. The value of ρ has been chosen based on previous experimental observations of the local structure of wormlike micelles [25] and on the fact that the uncharged model describes the structure and EV effects of both wormlike micelles and polystyrene in a good solvent [22,25]. The continuous limit in the model is obtained by letting $N \to \infty, a \to 0$, and $\theta \to 0$, with the constraint that L and b remain constant. Only in the single-chain simulations have we extrapolated to the continuous limit. The procedure consists in performing for each value of L/b a number of runs using different values of N and n_b and extrapolating the quantities of interest in the limit of $n_b^{-1} \to 0$. Here n_b denotes the number of spheres per Kuhn length, $n_b = b/a$, thus $L/b = N/n_b$. Typical values for N and n_b used range from 720 to 11 520 and from 3 to 192, respectively. In the many-chain simulations the large size of the systems studied makes practically unfeasible the use of such long chains, and therefore no continuous limit has been performed. We used in these simulations $n_b = 6$.

The electrostatic interactions are included by associating Z_b charges per Kuhn length. We have chosen to use $Z_b = 25$, 50 and 75, which is a value that should closely correspond to the situation encountered in our experiments with polymer-like micelles [5]. We do not take into account explicitly the presence of coions and counterions in this study: the only electrostatic interactions are those between fixed charges on the polyion, screened by clouds of coions of the added salt and counterions. This is mathematically expressed by the 'crude' approximations of the (Debye–Hückel) Coulomb interaction energy:

$$U(r) = \begin{cases} \dfrac{(Z_b L e/Nb)^2}{4\pi\epsilon_0\epsilon_r}\,\dfrac{e^{-r/\lambda_D}}{r} & \text{for} \quad r > 2\rho \\ \infty & \text{otherwise.} \end{cases}$$

In the above expression e is the elementary charge, ϵ_0 the permittivity of vacuum, ϵ_r the dielectric constant of the solvent and λ_D the Debye screening length. The solvent is treated as

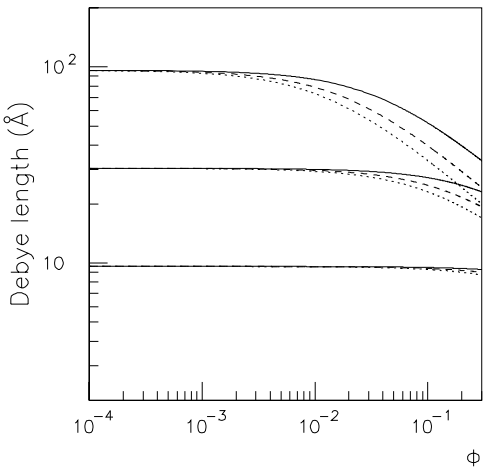

Figure 1. Debye length versus volume fraction Φ at different values of ionic strength I and charge density Z_b. From top to bottom: $I = 0.001$ M, $Z_b = 25, 50, 75$; $I = 0.01$ M, $Z_b = 25, 50, 75$; $I = 0.1$ M, $Z_b = 25, 50, 75$.

a dielectric continuum with a dielectric constant $\epsilon_r = 78.5$ (H_2O at 25 °C), assumed constant at all concentrations. The free ions in solution give rise to a screening length

$$\lambda_D = \left(\frac{\epsilon_0 \epsilon_r k_B T}{2e^2 I}\right)^{1/2} \tag{2}$$

where k_B is Boltzmann's constant, T the absolute temperature and I the ionic strength in mol l^{-1} of the added salt. At infinite dilution I does not contain any contribution from the counterions but only from the added salt ions. At finite concentrations, in contrast, a significant contribution to I might arise from the presence of counterions in solution, and λ_D turns out to be a function of Φ, whose behaviour is sketched in figure 1. For more details on the model see [26, 27], and references therein.

During the simulation the end-to-end distance

$$D_{ee} = \left[\langle (\boldsymbol{R}_N - \boldsymbol{R}_1)^2 \rangle\right]^{1/2} \tag{3}$$

with $\boldsymbol{R}_i$ being the positions of the beads, and the radius of gyration

$$R_g = \left[\left\langle \frac{1}{N}\sum_{i=1}^{N} (\boldsymbol{R}_i - \boldsymbol{R}_{CM})^2 \right\rangle\right]^{1/2} \tag{4}$$

where $\boldsymbol{R}_{CM}$ is the position of the centre of mass of the chain, given by

$$\boldsymbol{R}_{CM} = \frac{1}{N}\sum_{i=1}^{N} \boldsymbol{R}_i \tag{5}$$

were sampled. In these expressions $\langle \cdots \rangle$ denotes the ensemble average. Statistical errors on the sampled quantities were determined by block analysis [28]. Trial configurations are accepted according to the Metropolis criterion [29].

We have also sampled the full system scattering function $S(q)$ and the single-chain scattering function $P(q)$, where q is the modulus of the scattering vector.

In the single-chain simulations trial chain configurations have been generated by means of the *pivot* [30, 31] algorithm, which is extremely efficient due to its very short correlation time for self-avoiding chains [32], even when screened electrostatic interactions are included [33].

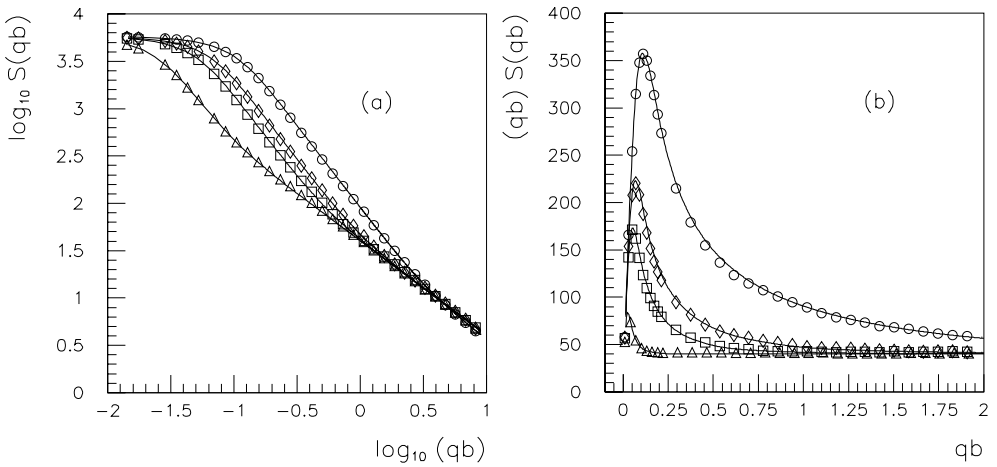

Figure 2. Example of scattering functions at infinite dilution at four different ionic strengths. The contour length is $L/b = 480$. The full curves are fits of the uncharged WLC function with EV as given in [22] to the MC data. Symbols: △, $I = 10^{-4}$ M; □, $I = 10^{-3}$ M; ◇, $I = 2.5 \times 10^{-3}$ M; ○, $I = 5 \times 10^{-2}$ M. (b) The same data as in (a) represented in a Holtzer plot, $qbS(qb)$ versus qb. Note that the point where the crossover occurs shifts toward lower values of q with decreasing ionic strength, as a qualitative demonstration of the increasing stiffness of the chain.

In the many-chain simulations the system is confined in a box with periodic boundary conditions. The side length of the box is chosen so that the desired volume fraction Φ is obtained: $L_{\rm box} = (V/\Phi)^{1/3}$, where $V = N_{\rm c}N4\pi\rho^3/3$ is an estimate of the volume of the $N_{\rm c}$ chains present. Trial configurations are generated by a reptation method. On increasing the chain concentration this algorithm increases its efficiency in comparison with the pivot. Note that the minimum q value sampled in the simulations is constrained to $q = 2\pi/L_{\rm box}$, and the minimum Debye length must be restricted to $\lambda_{\rm D} \ll L_{\rm box}$.

3. Single-chain simulations: results

3.1. Scattering function and Kuhn length

Examples of simulation results for the scattering functions are shown in figure 2. The fits (full curves) are performed using a numerical parametrization of the scattering functions for uncharged semiflexible chains with EV effects [22], treating the Kuhn length $b_{\rm tot}(n_b)$ as a fitting parameter so that the electrostatic contribution $b_{\rm el}(n_b)$ on this parameter is determined. It is remarkable that the scattering function of both uncharged and charged systems exhibits the same functional form, as the good quality of the fits demonstrates. Even the Holtzer plot (figure 2(b)), that is particularly sensitive to small deviations in the crossover region, shows very good agreement at all values of L and I investigated. From these fits we obtain an effective electrostatic Kuhn length $b_{\rm el}(n_b)$. After performing extrapolations to the limit $n_b \to \infty$ and $L \to \infty$ [26], we obtain the results plotted in figure 3 as $b_{\rm el}$ versus ionic strength I. We clearly see the increasing influence of electrostatic interactions on chain flexibility already apparent from the changes of the scattering curves in figure 2.

We can compare the simulation results with the predictions of the theoretical Odijk–Skolnick–Fixman (OSF) model [34]. The OSF theory splits the total Kuhn length into two

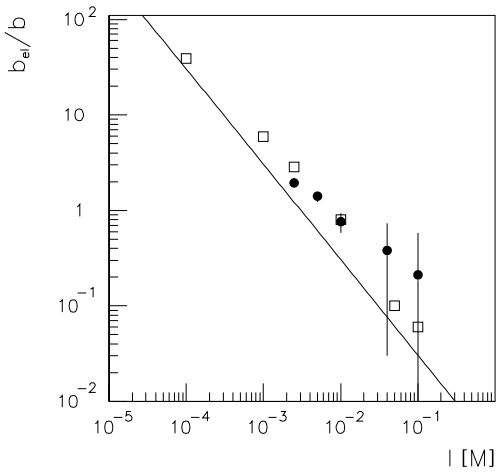

Figure 3. Electrostatic Kuhn length b_{el}/b versus chain length, extrapolated to the continuous limit of the model, and to $L \to \infty$, compared with the OSF prediction (full line). Symbols: MC data (□), experimental data (●).

contributions,

$$b_{tot} = b + b_{el} \tag{6}$$

where b is the Kuhn length due to the intrinsic stiffness of the chain and b_{el} is the electrostatic contribution, which for an infinitely long chain is given by

$$b_{el}^{\infty}(I) = \frac{\lambda_B}{2}\left(\frac{\lambda_D}{d}\right)^2 \tag{7}$$

where d is the distance apart of two neighbouring charges and

$$\lambda_B = \frac{e^2}{4\pi\epsilon_o\epsilon_r k_B T} \tag{8}$$

is the Bjerrum length. In figure 3 the MC data are compared with the theoretical expectations of the OSF theory (full line in the plot). One of the basic assumptions of the OSF theory is that the PEL is near to the rigid rod limit and, in fact, we notice that at low ionic strength, i.e. for increasing stiffness of the chain, the MC results converge asymptotically to the OSF values. However, in the range of I investigated b_{el} does not show the simple scaling (power law) predicted. The occurrence of more complex scaling has been also pointed out theoretically by means of variational calculations, for example in the work of Ha and Thirumalai [35].

The MC data can also be compared with our experimental neutron scattering results on dilute mixtures of the nonionic surfactant $C_{16}E_6$ and small amounts (6 wt%) of the ionic surfactant $C_{16}SO_3Na$ in a NaCl solution, which form PEL-like wormlike micelles. In the experiments the total Kuhn length was determined by a least-squares fit of the scattering data using the same fitting model as in the simulations. For a fixed value of the ionic strength, experiments have been performed at different concentrations of the solution. We have observed a significant dependence of the total Kuhn length on the concentration, which is ascribed to interchain interactions [4]. The data shown in figure 3 are linear extrapolations of b_{tot}/b to zero concentration. The complete experimental investigation is reported in [5]. Figure 3 provides us with a qualitative verification of the previously suggested analogy between PELs and polymer-like nonionic micelles doped with a small amount of an ionic surfactant. As discussed before,

in these systems we can profit from the much higher scattering contrast of wormlike micelles when compared with classical PELs, that enables us to perform experiments in dilute solutions and to obtain a higher accuracy in the determination of $b_{\rm tot}$ from an analysis of scattering curves. We find excellent agreement between the simulation and experimental data.

3.2. Radius of gyration

The radius of gyration of ideal WLC has been calculated by Benoit–Doty [36] under very general assumptions

$$\langle R^2_{\rm g,0}\rangle = \frac{1}{6}Lb - \left(\frac{b}{2}\right)^2 + \frac{b^3}{4L}\left(1 + \frac{b}{2L}(\mathrm{e}^{-2L/b} - 1)\right). \tag{9}$$

Thus, $R_{\rm g}$ written in units of the Kuhn length turns out to be a function of the ratio L/b only

$$\langle R_{\rm g,0}\rangle/b = f_{\rm BD}(L/b) \tag{10}$$

where

$$f_{\rm BD}(L/b) = \left[\frac{L}{6b} - \frac{1}{4} + \frac{b}{4L}\left(1 + \frac{b}{2L}(\mathrm{e}^{-2L/b} - 1)\right)\right]^{1/2}. \tag{11}$$

The scaling expressed by equation (10), which in the case of ideal chains is a direct consequence of the Benoit–Doty relation, assumes a deeper meaning in the presence of electrostatic interactions and EV. This is demonstrated in figure 4(a), where the MC data, plotted in units of $b_{\rm tot}$ versus $L/b_{\rm tot}$ for different values of I, collapse on a single master curve $g(L/b_{\rm tot})$. This proves that the scaling (10) is also preserved in the presence of interactions, provided that b is replaced with $b_{\rm tot}$, i.e. an additional contribution to the intrinsic Kuhn length is included. In a next step we can address the exact form of g by recalling that the increase of the radius of gyration can be expressed in terms of the *expansion factor* [37]

$$\alpha^2_{\rm g} = \frac{\langle R^2_{\rm g}\rangle}{\langle R^2_{\rm g,0}\rangle}. \tag{12}$$

Pedersen *et al* [38] have analysed the dependence of $R_{\rm g}$ on the chain length for neutral systems with EV interactions, by MC simulations. The authors have found the empirical expression for the expansion factor

$$\alpha^2(x) = \left[1 + \left(\frac{x}{c_1}\right)^2 + \left(\frac{x}{c_2}\right)^3\right]^{\epsilon/3} \tag{13}$$

where $x = L/b$, to fit the MC data in the full range of L/b simulated (up to $\approx$18 000) very well (for details, and for the numerical values of the constants in equation (13), see the above reference). Since α and $f_{\rm BD}(L/b_{\rm tot})$ give the contribution to the expansion due to non-local effects (EV) and to the increased local flexibility, respectively, we found it interesting to compare, in figure 4(a), the quantity $\alpha(L/b_{\rm tot})f_{\rm BD}(L/b_{\rm tot})$ (broken curve) with the MC data. The very good agreement observed allows us to assume that

$$g(L/b_{\rm tot}) = \alpha(L/b_{\rm tot})f_{\rm BD}(L/b_{\rm tot}). \tag{14}$$

This result demonstrates the consistency of our simulation results with the general OSF approach, which treats interaction between neighbouring charges as a local effect that produces an increase in the Kuhn length of the chain, and to incorporate those between charges located far apart along the chain into EV effects. We stress that α in equation (14) is exactly the expansion factor of chains without electrostatic interactions, but with L rescaled with $b_{\rm tot}$.

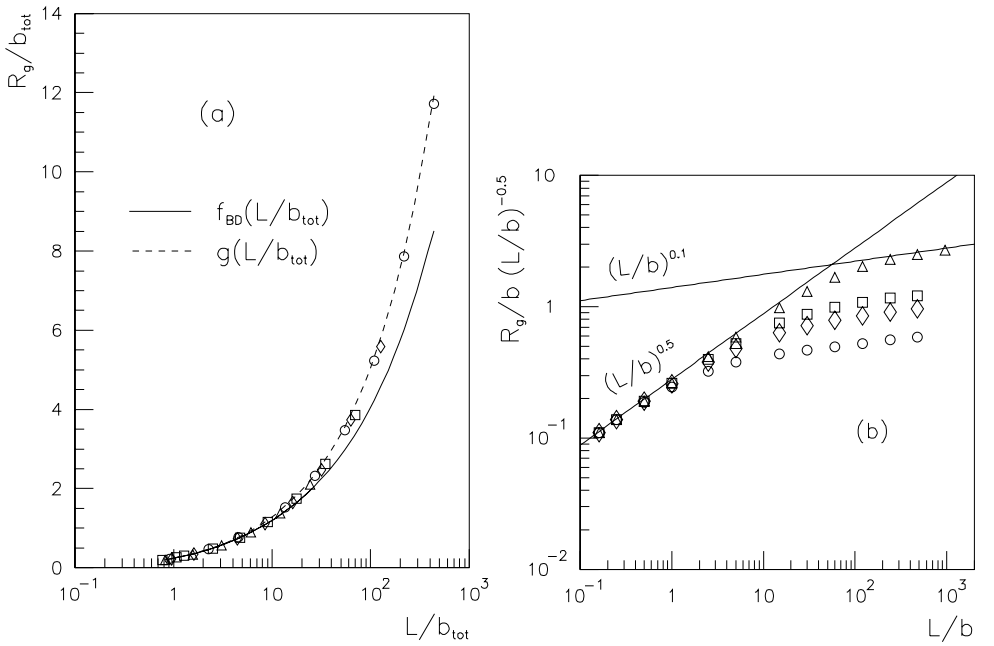

Figure 4. (a) Radius of gyration data collapsing observed after rescaling all lengths by b_{tot}. (b) Radius of gyration in unit of b versus L/b (cf figure 2 in [39]). Symbols: the same as in figure 2.

Note that if the contour length is known, equation (14) can be used to determine the total Kuhn length from experimental or simulation data.

We have also compared our data with a recent variational calculation of Ghosh *et al* [39]. In the attempt to make such a qualitative comparison easier, we have re-plotted our data in figure 4(b) using the same units as in figure 2 of [39]. Both MC data and variational calculations exhibit the same behaviour: at short chain lengths the rigid-rod behaviour is encountered. On increasing L/b a crossover region is entered without a simple power law scaling. At even larger contour lengths the self-avoiding regime is reached. Note that our chains are not long enough to fully enter this regime.

4. Many-chain simulations: results

4.1. Scattering function and related quantities

Examples of MC results of the scattering function at different volume fractions are displayed in figure 5. Two main effects are evident. At all ionic strengths, as well as for the uncharged system, $S(0)$ decreases with increasing concentration due to inter-chain interactions. As expected, this effect is much more pronounced when the electrostatic interactions are stronger, i.e. at lower ionic strength and at higher charge density. Physically, this corresponds to an increase of the osmotic compressibility of the system. For strongly interacting chains a peak in $S(q)$ is observed. This is a well known feature also observed in experiments and indicates local ordering in the system. On increasing concentration, the peak position moves toward higher scattering vectors, as the chains are on average closer to each other. A similar shift of the peak position is observed at fixed Φ and with increasing I. In this case the decrease of d is due to the weakening of the electrostatic repulsion as the screening is increased, and therefore chains are allowed to come closer.

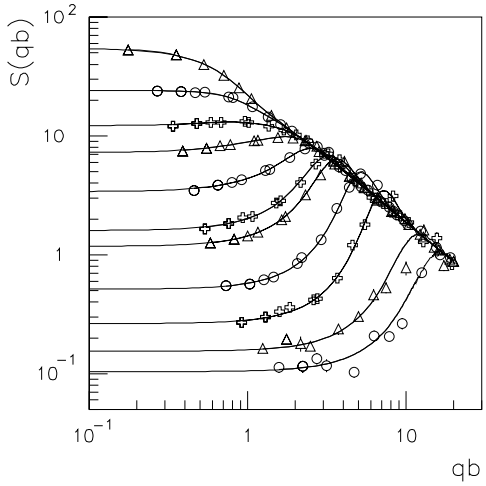

Figure 5. Effects of concentrations on the scattering function $S(q)$ at $Z_b = 50$, and $I = 0.001$ M: from top to bottom $\Phi = 10^{-4}$, 0.001, 0.002, 0.003, 0.005, 0.008, 0.01, 0.02, 0.04, 0.1, 0.2. Full lines: fits (see [27]).

Based on the PRISM theory [40], a method to fit $S(q)$ in the whole range of q and at all settings of the other parameters used in the simulations has been developed in [27]. The fitted $S(q)$ curve allows one to determine $S(0)$, and the position of the peak, when present.

4.2. Position of the peak of $S(q)$

A quantitative analysis of the peak position q^* is worthwhile, since it can be directly compared with experimental results and theories. Figure 6 contains plots of q^* derived from MC data as described in the previous section. q^* is displayed versus Φ at $I = 10^{-3}$ M and at $Z = 25$, 50 and 75. At high enough concentrations q^* is found to scale as $\sim \Phi^{1/2}$. This is predicted from most theories [41], and also reported in many experimental works. In figure 6 we also compare the MC data with our previous experimental results on a mixture of non-ionic surfactant and 3 or 6% of ionic surfactant [5]. The MC data reproduce the correct scaling exponent, and also the position of the crossover at low concentration. Only the non-universal prefactor is, probably, slightly different. The agreement shows that the simple model adopted in the simulations is able to reproduce general properties of the investigated system.

4.3. Scaling of the forward scattering

An important quantity to consider is the forward scattering, because it is directly related to the osmotic compressibility Π of the system through [41]

$$S(0) = k_{\mathrm{B}}T \left(\frac{\mathrm{d}\Pi}{\mathrm{d}c} \right)^{-1}. \tag{15}$$

Figure 7(a) shows the values of $S(0)$ obtained by fitting the total scattering function, as described in section 4.1. In order to find a possible universal behaviour of $S(0)$, we recall that $S(0)$ data of uncharged systems, corresponding to different values of b and L, collapse on a single curve if plotted against the reduced concentration $\tilde{c} \propto c/c^*$, where $c^* \sim R_{\mathrm{g}}^{-3}$ is the overlap concentration. In the presence of Debye–Hückel interactions the Debye length appears

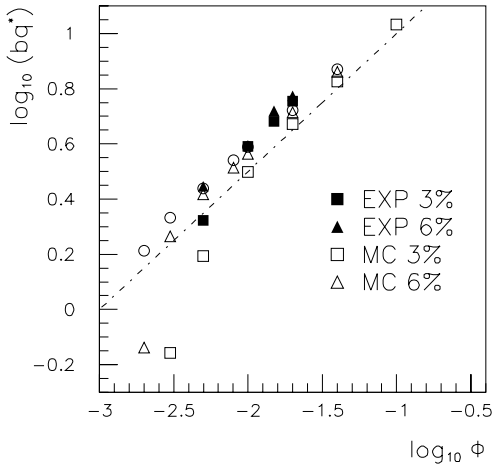

Figure 6. Comparison of the peak position of $S(q)$ from simulation data, at $I = 0.001$ M, $Z_b = 25$ (□), 50 (△), 75 (○), with experimental data on $C_{16}E_6$ doped with 3% ionic surfactant $C_{16}SO_3Na$ (■), and with 6% of ionic surfactant (▲). The straight line has a slope of 1/2, that is the value theoretically predicted.

as a characteristic length, in addition to the effective hard-sphere radius ρ, which mimics the EV effects. Two effects have now to be taken into account: the swelling of the chains due to increased stiffness and the increase of the EV effect. In rescaling the volume fraction, we have tried to take into account the first effect by replacing R_g with the sampled radius of gyration $R_g(I, Z_b)$ in the presence of charges, added salt, and at infinite dilution, while the second effect is included by replacing ρ with $\rho + \lambda_D$. We have therefore found it reasonable to define a rescaled volume fraction for charged systems as

$$\Phi_r = \left(\frac{\lambda_D + \rho}{\rho}\right)^{\delta} \left(\frac{R_g(I, Z_b)}{R_{g,u}}\right)^3 \Phi \tag{16}$$

where $R_{g,u}$ is the radius of gyration of the uncharged chain at infinite dilution. In figure 7(b) we plot the MC data of $S(0)$ versus Φ_r. The data are found to follow a master curve very closely if $\delta = 1$ is assumed. At high values of Φ deviations are found, analogous to what is reported for similar MC simulations on uncharged systems [23]. This is not surprising considering that equation (16) does not account for screening of EV effects at high concentration. Nevertheless, the simple behaviour of (16) provides us with a straightforward interpretation: electrostatic interactions on $S(0)$ can in some respect be accounted for through a simple increase of the EV strength, and of the stiffness of the chain. The full curve in figure 7(b) is a fit obtained using a modified renormalization group calculation of Otha and Ono [42] for uncharged polymers (for details see [27]). The main result is the scaling $S(0) \sim \Phi^{-\tau}$ in the semidilute regime, with $\tau \simeq 1.8$.

Before concluding we wish to give an example of a possible application of the scaling law of $S(0, \Phi_r)$ found to determine the growth law for charged wormlike micelles by means of experimental data. The forward scattering and the apparent molar mass are related through

$$M_{app} = \langle M \rangle_W \, S(0, \Phi_r) \tag{17}$$

where $\langle M \rangle_W$ is the weight-average molar mass [43]. Assuming a power law for the molecular weight

$$\langle M \rangle_W = B c^{\alpha} \tag{18}$$

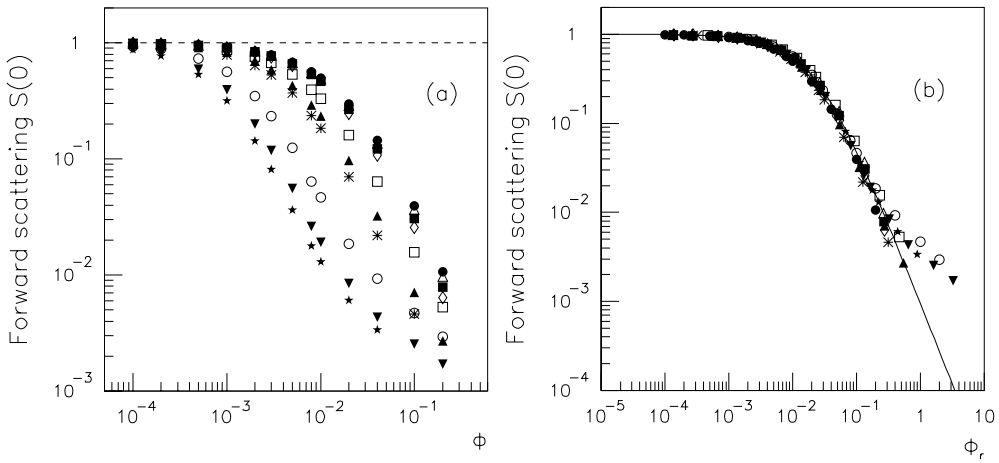

Figure 7. (a) Data for the forward scattering $S(0)$ versus Φ, for all sets of simulations. (b) Collapsing of the data in (a) when plotted versus the rescaled volume fraction Φ_r defined by (16), with $\delta = 1$. Full curve: renormalization group calculation of Otha and Ono, employed with a generalized exponent. In the semidilute regime the scaling is $S(0) \sim \Phi_r^{-1.8}$. Symbols: uncharged chains (●); $Z_b = 25$, $I = 0.1$ M (△), $I = 0.01$ M (□), $I = 10^{-3}$ M (○); $Z_b = 50$, $I = 0.1$ M (■), $I = 0.01$ M (▲), $I = 10^{-3}$ M (▼); $Z_b = 75$, $I = 0.1$ M (◇), $I = 0.01$ M (∗), $I = 10^{-3}$ M (⋆).

where c is the concentration, the right-hand side of equation (17) can be expressed in terms of the two unknown quantities B and α. $M_{\rm app}$ can be measured, e.g. by static light scattering experiments, and B and α can be obtained by fitting equation (17) to the experimental data, provided that a functional form for $S(0, \Phi)$ exists (see [3, 44] for uncharged micelles).

5. Conclusions

The effects of electrostatic and EV interactions on size, flexibility and scattering functions of charged semiflexible chains have been analysed by MC simulations, and compared with experimental findings on charged wormlike micelles, and with existing theories.

At infinite dilution we have shown that the scattering functions can be fitted by the WLC model of an uncharged chain with EV. The fits allowed an accurate determination of the total Kuhn length, which includes the effects of electrostatic interactions. The results are in excellent agreement with the Kuhn length determined for charged wormlike micelles under similar conditions as used in the simulations. Both sets of results are in reasonable agreement with the classical OSF theory; however, the observed Kuhn length is slightly larger than predicted. MC simulations are also found to be in qualitative agreement with more recent variational calculations.

Plotting the radius of gyration as a function of the contour length in units of the total Kuhn length makes the data for different ionic strengths collapse on the same curve. This universal behaviour is in fact the same as that found for neutral semiflexible chains with EV interactions. Again, the data are in qualitative agreement with variational calculations.

At finite concentration, when interchain interactions are strong enough, the many-chain scattering function shows the characteristic structural peak, as observed in many experiments. Using a fit function based on the PRISM theory, it was possible to fit the $S(q)$ in the full range of the scattering vector, and to determine the forward scattering and the position of the peak.

After plotting $S(0)$ versus a rescaled concentration Φ_r the data collapse on a single master curve. This remarkable property shows that, within the approximation used, the effect of the electrostatic interactions on the osmotic compressibility can be accounted for by an increase of the EV strength and of the stiffness of the chains. In the semidilute regime $S(0)$ decays with a power law with an exponent $\sim$1.8. At higher Φ, when the chains enter the ideal regime, deviations in the scaling plot show up.

The analysis of the position of the peak shows excellent agreement with both experiments and theory. In particular, the MC data reproduce the results of our experiments on charged wormlike micelles very well.

Despite the severe approximations of the *continuous model* used, general properties of the simulated systems such as the Kuhn length and the position of the peak are found to agree with experiments. It is clear that our data have been obtained under conditions where the approximations made should be appropriate. However, it is also clear that we are now in a position to compare experimental scattering data of a quality far superior to those obtained with classical PEL with simulated scattering functions.

We have in this work taken the first steps in the direction of providing a fitting function which can be used in the analysis of our light scattering and SANS data on charged wormlike micelles [5]. We now have numerical expressions for $S(0)$ which can be used in attempts to determine the growth laws of the micelles from the forward scattering as determined by light scattering. We have furthermore expressions [27] which will allow us to aim at fitting the full q range of the measured scattering data. In this procedure the variation of the Kuhn length with concentration and ionic strength as determined by the simulations should be employed together with the knowledge of $S(0)$ and the growth law, which we hope we can determine from the analysis of the light scattering data, and will be the object of a forthcoming publication.

Acknowledgment

The financial support of the Swiss National Science Foundation (grant no 20-53381.98 and no 20-46627.96) is gratefully acknowledged.

References

[1] Cates M E and Candau S J 1990 *J. Phys.: Condens. Matter* **2** 6869
[2] Magid L J 1998 *J. Phys. Chem.* B **102** 4064
[3] Schurtenberger P and Cavaco C 1993 *J. Physique* II **3** 1279
Schurtenberger P and Cavaco C 1994 *J. Phys. Chem.* **98** 5481
Schurtenberger P and Cavaco C 1994 *Langmuir* **10** 100
Schurtenberger P, Cavaco C, Tiberg F and Regev O 1996 *Langmuir* **12** 2894
[4] Jerke G, Pedersen J S, Egelhaaf S U and Schurtenberger P 1998 *Langmuir* **14** 6013
[5] Sommer C, Cannavacciuolo L, Egelhaaf S U, Pedersen J S and Schurtenberger P 2000 *Prog. Colloid Polym. Sci.* **115** 347
Sommer C, Pedersen J S, Egelhaaf S U, Cannavacciuolo L, Kohlbrecher J and Schurtenberger P *Langmuir* at press
[6] For a review, see, for example, Dautzenberg H, Jaeger W, Kötz J, Philipp B, Seidel Ch and Stscherbina D 1994 *Polyelectrolytes: Formation, Characterization and Applications* (Munich: Hanser)
Schmitz K S *Macro-Ion Characterization: from Dilute Solution to Complex Fluid (ACS Symp. Series Vol. 548)* (Washington, DC: ACS)
Förster S and Schmidt M 1995 *Adv. Polym. Sci.* **120** 50
Barrat J L and Joannny J F 1996 *Adv. Chem. Phys.* **XCIV** 1
[7] Carnie S L, Christos G A and Creamer T P 1988 *J. Chem. Phys.* **89** 6484
[8] Carnie S L, Christos G A and Creamer T P 1992 *Macromolecules* **25** 1121
[9] Hooper H H, Blanch H W and Prausnitz J M 1990 *Macromolecules* **23** 4820

[10] Reed C H and Reed W F 1991 *J. Chem. Phys.* **94** 8479
[11] Micka U and Kremer K 1996 *J. Phys.: Condens. Matter* **8** 9463
[12] Micka U and Kremer K 1997 *Europhys. Lett.* **38**
[13] Ullner M, Jönsson Bo, Peterson C, Sommelius O and Söderberg Bo 1997 *J. Chem. Phys.* **107** 1279
[14] Carnie S L and Christos G A 1990 *J. Chem. Phys.* **92** 7661
[15] Stevens M J and Kremer K 1996 *J. Physique II* **11** 1607
[16] Stevens M J and Kremer K 1995 *J. Chem. Phys.* **103** 1669
[17] Stevens M J and Kremer K *Macro-Ion Characterization: From Dilute Solution to Complex Fluid (ACS Symp. Series Vol. 548)* ed K S Schmitz (Washington, DC: ACS)
[18] Stevens M J and Kremer K 1993 *Phys. Rev. Lett.* **71** 2228
[19] Stevens M J and Kremer K 1993 *Macromolecules* **26** 4717
[20] Kremer K, Dünweg B and Stevens M J 1993 *Physica A* **194** 321
[21] Binder K 1995 *Monte Carlo and Molecular Dynamics Simulations in Polymer Science* (Oxford: Oxford University Press)
[22] Pedersen J S and Schurtenberger P 1996 *Macromolecules* **29** 7602
[23] Pedersen J S and Schurtenberger P 1999 *Europhys. Lett.* **45** 666
[24] Kratky O and Porod G 1949 *Rev. Trav. Chim.* **68** 1106
[25] Schurtenberger P, Scartazzini R, Magid L J, Leser M E and Luisi P L 1990 *J. Phys. Chem.* **94** 3695
Schurtenberger P, Magid L J, King S M and Linder P 1991 *J. Phys. Chem.* **95** 4173
Pedersen J S, Egelhaaf S U and Schurtenberger P 1995 *J. Phys. Chem.* **99** 1299
[26] Cannavacciuolo L, Sommer C, Pedersen J S and Schurtenberger P 2000 *Phys. Rev.* E **62** 5409
[27] Cannavacciuolo L, Pedersen J S and Schurtenberger P *Langmuir* submitted
[28] Flyvbjerg H and Petersen H G 1989 *J. Chem. Phys.* **91** 461
[29] Metropolis N, Rosenbluth A W, Rosenbluth A H, Teller A H and Teller E 1953 *J. Chem. Phys.* **21** 1087
[30] Stellman S D and Gans J P 1972 *Macromolecules* **5** 516
[31] Seidel C, Schlaken H and Müller I 1994 *Macromol. Theory Simul.* **3** 333
[32] Madras N and Sokal A D 1998 *J. Stat. Phys.* **50** 109
[33] Seidel C 1996 *Ber. Bunsenges. Phys. Chem.* **100** 757
[34] Odijk T 1997 *J. Polym. Sci., Polym. Phys.* **15** 477
Skolnick J and Fixman M 1997 *Macromolecules* **10** 944
[35] Ha B-Y and Thirumalai D 1999 *J. Chem. Phys.* **110** 7533
[36] Benoit H and Doty P 1995 *J. Phys. Chem.* **57** 958
[37] Yamakawa H 1971 *Modern Theory of Polymer Solutions* (New York: Harper and Row)
[38] Pedersen J S, Laso M and Schurtenberger P 1996 *Phys. Rev.* E **54** R5917
[39] Ghosh K, Carri G A and Muthukumar M 2001 *J. Chem. Phys.* **115** 4367
[40] Schweizer K S and Curro J G 1987 *J. Chem. Phys.* **87** 1842
[41] Förster S and Schmidt M 1995 *Adv. Polym. Sci.* **120** 50
[42] Otha T and Ono Y 1982 *Phys. Lett.* A **89** 460
[43] Goodstein D L 1985 *States of Matter* (New York: Dover)
[44] Jerke G, Pedersen J S, Egelhaaf S U and Schurtenberger P 1997 *Phys. Rev.* E **56** 5772
Stradner A, Glatter O and Schurtenberger P 2000 *Langmuir* **16** 5345